06

Correlation of X-ray, TEM, and Raman Methods in the Study of Orientational Disorder in Multi-Walled Carbon Nanotubes

© N.G. Bobenko, V.E. Egorushkin, A.N. Ponomarev

Institute of Strength Physics and Materials Science, Siberian Branch, Russian Academy of Sciences,
634055 Tomsk, Russia
e-mail: nlitvin86@mail.ru

Received December 19, 2024
Revised December 19, 2024
Accepted December 19, 2024

The effect of mechanical grinding on the structure of multi-walled carbon nanotubes (MWCNTs) with diameters of 7 nm and 18 nm was investigated using X-ray diffraction (XRD), Raman spectroscopy, and transmission electron microscopy (TEM). The results demonstrated that for 7-nm nanotubes, grinding does not cause significant changes in lattice parameters or crystallite sizes, indicating preservation of the original structure. In contrast, 18-nm samples exhibited substantial structural changes, including reduced interlayer spacing and peak splitting in Raman spectra, suggesting the formation of torsional deformations due to layer rotations relative to one another. The integrated approach combining XRD, TEM, and Raman spectroscopy revealed correlations between mechanical grinding conditions and structural changes, which are crucial for tailoring MWCNT properties for various applications such as catalysis and composites.

Keywords: Multi-walled carbon nanotubes, microstructure, Raman spectroscopy, TEM, X-ray diffraction.

DOI: 10.61011/TP.2025.05.61122.452-24

Introduction

Multi-walled carbon nanotubes (MWCNTs) are a materials whose properties — such as chirality, diameter, number of layers, type and density of defects, length, etc. — are determined by their structure. These parameters determine the potential applications of MWCNTs in various fields [1–3] The structure of MWCNTs is formed both in the synthesis stage and during post-processing [4]. Mechanical treatment, including grinding in a planetary mill, results in MWCNTs being cut into smaller fragments, narrowing of their length distribution, and an increase in their specific surface area [5,6]. These structural changes are particularly beneficial for the application of MWCNTs in catalysis, composite materials, and biomedicine, where a high specific surface area and short diffusion paths are required [3,7–9].

The structure of MWCNTs after grinding is determined by the processing conditions and the synthesis method. X-ray diffraction analysis (XRD) is one of the most effective methods for studying the structure of MWCNTs. This method enables accurate determination of lattice parameters, identification of impurities, and calculation of coherent domain sizes [10]. XRD is widely used to evaluate synthesis quality and to study structural changes and directional stresses arising during synthesis and post-processing. For example, in [11] it was shown that XRD peaks for single-walled carbon nanotubes are significantly broadened compared to those for MWCNTs. In [12], it was found that for MWCNTs of various diameters obtained by chemical vapor deposition, both the internal stresses and coherent domain sizes depend on the nanotube diameter.

Raman spectroscopy is a valuable complement to XRD. It may be used to determine the number and type of defects, the degree of graphitization, and the size of MWCNTs crystallites [13]. Peaks D and G, as well as their splitting, provide data on disorder in carbon layers. In [14], it was shown that Raman spectroscopy detects functional groups on the surface of nanotubes and determines the chirality type of single-walled carbon nanotubes.

Transmission electron microscopy (TEM) is an indispensable tool for studying the morphology and interlayer distances in MWCNTs. This method allows visualization of the nanotube structure and records the distortions induced during their processing. For example, TEM reveals orientational changes, such as the appearance of moir-patterns, in double-walled nanotubes. Based on TEM images, torsional deformations in graphite after mechanical grinding were observed, confirming the importance of TEM for structural investigations. The collective effect of the structural changes described above leads to the formation of orientational disorder in nanocarbon materials.

Despite practical interest in structural changes during mechanical grinding of MWCNTs, existing studies are often limited to specific parameters, such as lattice constants or defects. It remains unclear how mechanical treatment affects interlayer distances, defect formation mechanisms, and the development of structural disorder, thus limiting a comprehensive understanding of structural changes in MWCNTs after processing.

In this work, MWCNTs with diameters of 7 and 18 nm were studied before and after mechanical grinding using X-ray diffraction, Raman spectroscopy, and TEM. Changes in

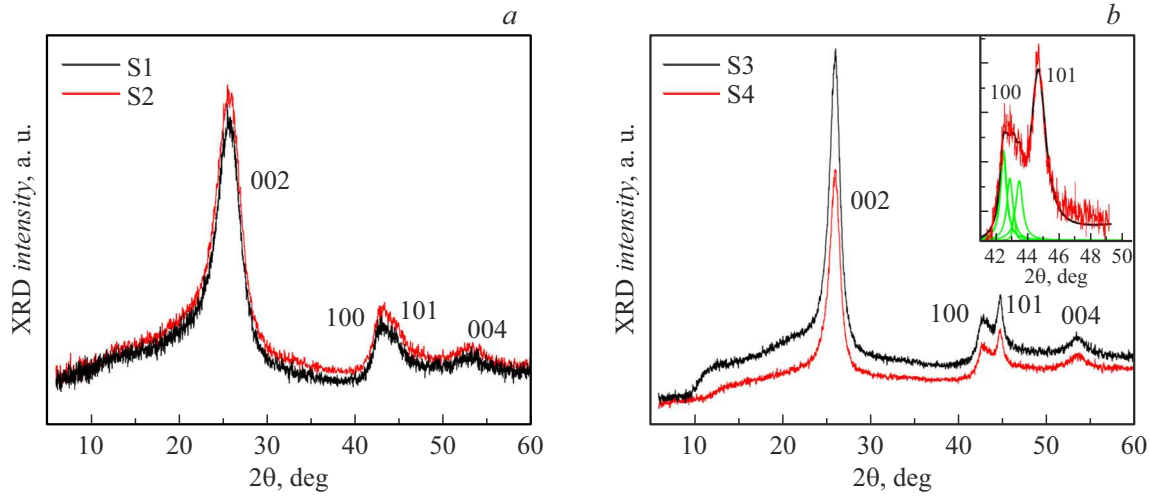

Figure 1. XRD patterns of samples S1, S2 (black and red curves, respectively) (*a*) and S3, S4 (black and red curves, respectively) (*b*). Inset: Lorentzian fitting of the (100) peak of sample S4.

lattice parameters, crystallite sizes, degree of graphitization, and interlayer distances were determined. In addition, structural distortions induced by mechanical grinding were identified.

1. Materials and methods

Nanotubes with diameters of 7 nm (samples S1 and S2) and 18 nm (samples S3 and S4) were chosen for studies of structural changes occurring in MWCNTs as a result of grinding. Samples S1 and S3 are as-prepared nanotubes, while S2 and S4 are nanotubes after grinding.

All MWCNTs were synthesized by chemical vapor deposition (CVD) with subsequent rinsing in a 15 % solution of HCl and distilled water to a neutral pH and drying in air [15].

To obtain samples S2 and S4, samples S1 and S3 were ground in an AGO-2 („Novic-mill, Russia“) planetary ball mill [16] with a ball diameter of 4 mm, a balls/powder weight ratio of 800 : 20, and a ball acceleration of 200 m/s^2 for 2 min.

All samples were studied by XRD and Raman spectroscopy. Additional TEM studies were performed for 18-nm samples. A PANalytical Empyrean diffractometer (Malvern Instruments, United Kingdom) with a CuKα_1, $\lambda p = 1.54056$ Å emitter was used for XRD. The crystallography open database (COD) was used to interpret the obtained XRD patterns. Raman spectra were measured at room temperature by an NT-MDT-Solar AFM/Raman spectrometer (NT-MDT, Moscow, Russia) at a laser wavelength of 633 nm. These spectra were fitted with Lorentzian functions in OriginPro 2022 (Academic). The linear sizes of crystallites (L_α) were calculated as $L_a = (2.4 \cdot 10^{-10})\lambda^4 \left(\frac{I_D}{I_G}\right)^{-1}$, where I_D, I_G are the intensities of peaks D and G, respectively [17].

The morphology of MWCNTs was examined using a Thermo Fisher Scientific Talos L120C TEM (Czech Republic) in the bright field mode at an accelerating voltage of 20–120 kV with a resolution of 0.37 nm at room temperature. Analysis and computer processing of digital electron microscopic images were performed in ImageJ.

2. XRD

The X-ray diffraction patterns of all samples are shown in Fig. 1. Miller indices, angles 2θ, broadening ΔB, and calculated lattice parameters determined by analyzing these patterns are listed in Table 1.

Lattice parameters were calculated using the relation between interplanar distance d_{hkl} and $\boldsymbol{a}$, $\boldsymbol{c}$: $d_{hkl} = \left(\frac{4(h^2+k^2+hk)}{3a^2} + \frac{l^2}{c^2}\right)^{-0.5}$ [18]. The value of d_{hkl} was calculated in accordance with the Wulff–Bragg formula: $2d_{hkl}\sin\theta = n\lambda$. Here, hkl are the Miller indices of a plane, θ is the scattering angle, n is the order of a maximum, and λ is the X-ray radiation wavelength. Parameters $\boldsymbol{a}$ and $\boldsymbol{c}$ were determined by analyzing peaks type (100) and (002), (004), respectively.

Diffraction peaks (002) at $2\theta \approx 26°$, (100) at $2\theta \approx 42.8°$, (101) at $2\theta \approx 44.7°$, and (110) are found in the patterns of all four samples and correspond to the hexagonal structure of graphite (according to COD 96-901-2231).

Broadening ΔB for peak (002) of MWCNTs with a diameter of 7 nm (samples S1 and S2) decreases by 0.65° after grinding. The positions of peaks (002) and (100) remain virtually unchanged. The as-prepared and ground nanotubes have the same values of lattice parameters $\boldsymbol{c} = 3.49$ Å and $\boldsymbol{a} = 2.45$ Å. All this is indicative of refinement of the crystal structure.

In the case of MWCNTs with a diameter of 18 nm, the positions of peaks (002) and interlayer distances calculated based on this peak ($\boldsymbol{c} \approx 3.43$ Å) match for S3 and S4.

Table 1. Characteristics of XRD patterns of samples S1–S4

hkl	Angles 2θ, degree		Broadening ΔB, degree		Lattice parameter, Å	
	S1	S2	S1	S2	S1	S2
002	25.531	25.80	2.97	2.32	$\boldsymbol{c} = 3.49$	3.49
100	42.84	42.97	1.29	1.52	$\boldsymbol{a} = 2.45$	2.45
101	44.71	44.83	1.98	2.22		
004	–	52.83	–	3.31	–	3.43
	S3	S4	S3	S4	S3	S4
002	25.95	25.94	1.47	1.43	$\boldsymbol{c} = 3.43$	3.43
100	42.84	42.53 42.92 43.16 43.50	1.09	0.48 0.30 0.16 0.42	$\boldsymbol{a} = 2.45$	2.45 2.43 2.42 2.40
101	44.71	44.61	1.27	1.09	–	–
004	53.42	54.1	2.05	1.64	$\boldsymbol{c} = 3.43$	3.38

The second-order (004) peak in S4 is shifted by 0.7° relative to the corresponding peak in S3. The interlayer distances calculated based on (004) for S3 and for S4 were $\boldsymbol{c} \approx 3.43$ Å and ≈ 3.38 Å respectively.

Peak (100) in S3 may be represented by a single Lorentzian; lattice parameter $\boldsymbol{a} \approx 2.45$ Å and distance $a_0 = \frac{a}{\sqrt{3}} = 1.42$ Å between carbon atoms in a layer (C–C-bond length) calculated for S3 based on this peak then match the graphene lattice parameter (1.42 Å) [19].

In sample S4, peak (100) is decomposed into four Lorentzians (inset in Fig. 1 *b*) with maxima positioned at 42.53°, 42.92°, 43.16°, and 43.50° (Table 1). Four different structures correspond to these maxima. The lattice parameters ($\boldsymbol{a}$) of these structures calculated as detailed above are 2.40, 2.42, 2.43, and 2.45 Å, while the lengths of C–C- bonds are 1.38, 1.40, 1.41, and 1.42 Å respectively. It is fair to assume that the sample is divided into blocks, and each of them is characterized by its own value of lattice parameters $\boldsymbol{c}$ and $\boldsymbol{a}$ in directions (h00) and (00l) [20]. Each „block" scatters X-rays independently and produces a diffraction maximum at a position corresponding to its lattice parameter value. Thus, the resulting maximum from the entire sample consists of four maxima corresponding to structures with different interlayer distances and bond lengths. A similar pattern is observed in turbostratic graphene [21]: different lattice parameters and C–C- bond lengths correspond to different rotation angles of layers. With this similarity taken into account, the spread of parameters $\boldsymbol{c}$ and $\boldsymbol{a}$ in S4 corresponds to a structure where the upper layer regions are rotated by $\sim 10°$ [22].

Thus, the grinding of MWCNTs with a diameter of 7 nm does not induce any significant changes in structural parameters. Nanotubes with a diameter of 18 nm undergo significant changes in lattice parameters, C–C- bond lengths, and interlayer distances, which may induce rotation of local regions of the carbon layer.

Table 2. I_D/I_G intensity ratio and calculated linear sizes L_a determined by analyzing the Raman spectra

Parameter	S1	S2	S3	S4
I_D/I_G	1.7	1.7	0.9	1.3
L_a, nm	23	23	41	29

3. Raman spectroscopy

The Raman spectra for MWCNTs with diameters of 7 and 18 nm before and after grinding are shown in Fig. 2. The spectra of samples S1, S3, and S4 feature *D*, *G*, and 2*D*-peaks. All peaks are normalized to the G-mode intensity. The I_D/I_G intensity ratio and calculated linear sizes L_a are presented in Table 2.

Peak *G* corresponds to vibrations of sp^2- carbon bonds and indicates the degree of graphitization of samples [23]. Peak *D*, which is associated with interplanar vibrations of atoms, is indicative of the presence of various structural defects [23]. Overtone peak 2*D*- of the G- mode is representative of distortion of the material crystallinity [24,25].

The grinding of samples with a diameter of 7 nm leads to a slight change in intensity and a shift of maxima of peaks *D*, *G*, and 2*D* toward higher frequencies, which may be attributed to compression of the carbon lattice [25]. Crystallite size $L_a = 23$ nm does not change in the process of grinding.

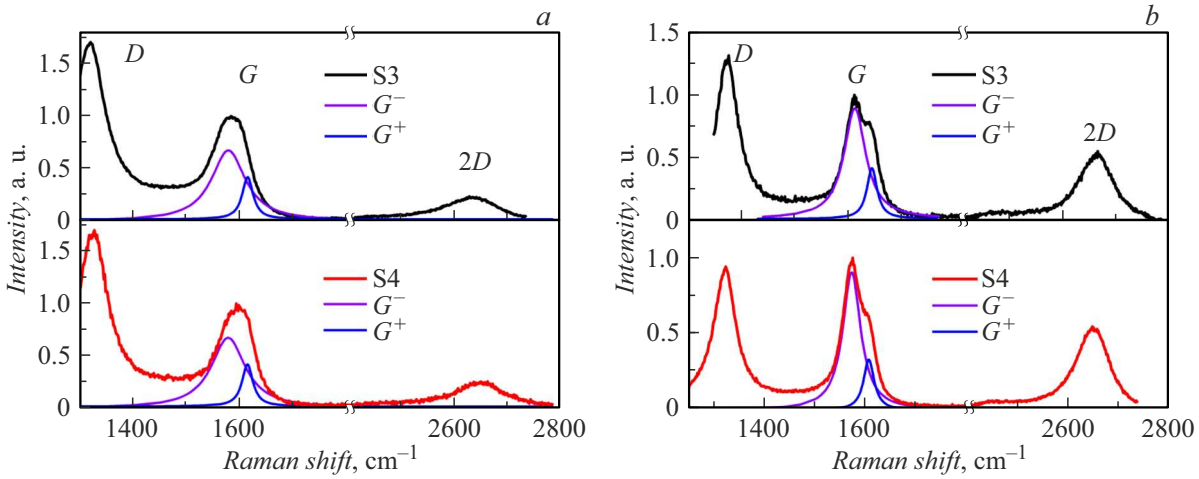

Figure 2. Raman spectra of samples S1, S2 (black and red curves, respectively) (*a*) and S3, S4 (black and red curves, respectively) (*b*). The decomposition of peak *G* into sub-peaks G^- (purple curve) and G^+ (blue curve) is shown in all panels.

Table 3. Positions (cm^{-1}) and relative integral areas (*S*) of Lorentzians G^-, G^+, and 2*D*

Sample No.	G^-		G^+		2*D*	
	cm^{-1}	*S*	cm^{-1}	*S*	cm^{-1}	*S*
S1	1571	19	1603	9	2634	9
S2	1580	20	1611	11	2646	14
S3	1573	28	1607	7	2646	26
S4	1580	25	1614	9	2655	23

The grinding of nanotubes 18 nm in diameter induces more significant changes. In the as-prepared sample (S3), the *G*- peak is higher than *D*. Following grinding, the *D*- peak intensity increases by $\sim 40\,\%$, peak *G* shifts, and crystallite size L_a decreases from 41 to 29 nm.

All the peaks of samples were decomposed into Lorentzians for in-depth analysis of the structure. Let us focus on the fitting of *G*- peaks (to identify changes in the graphite sample component) and peak 2*D*- (to obtain additional data on structural defects; see Table 3). The *G*- peak is split into G^- and G^+ components in all four samples. This splitting in MWCNTs with a diameter of 7 nm is caused by interlayer interactions [26–28]. Peaks G^- and G^+ become more intense after grinding of MWCNTs. All this is indicative of ordering of the structure after grinding.

Peak *G* for all MWCNTs with a diameter of 18 nm is also split. Grinding leads to suppression of G^- and intensification of G^+. The changes of G^- and G^+ in S4 are indicative of distortions, which are associated with rotation of the upper layer regions of a nanotube relative to the remaining layers, and the emergence of AB- regions alongside the initial AA ones (a similar pattern is observed in turbostratic graphene [29]). The angle of rotation of a layer relative to the initial AA- structure in sample S3 may be determined by comparing the shift of the 2*D*- peak in sample S4 relative to S3, the magnitude of splitting of the *G*- peak, and the linear size of a split crystallite and the size of a supercell in turbostratic graphene [30]. The magnitude of splitting of peak *G* in S4 matches that of the *G*- peak at an angle of $\sim 10^\circ$ in turbostratic graphene [30]. The 2*D*- peak in S4 is shifted by 9 cm^{-1} relative to its position in S3. This shift also corresponds to rotation of the upper layer in turbostratic graphene by an angle of $\sim 10^\circ$ [29].

Linear size $L_{cell} = 29.71$ nm of a supercell of turbostratic bigraphene with a rotation angle of $\sim 10^\circ$ [22] corresponds to crystallite size $L_a = 30$ nm for S4. Thus, the agreement between all these parameters indicates that the rotation angle of the upper layer regions in S4 is on the order of 10°.

4. TEM

Additional comparative analysis of TEM images of samples S3 and S4 was performed in order to verify the XRD and Raman spectroscopy data on differences in interlayer distances and the emergence of local rotations of the upper layer in S4. Figure 3 presents the TEM images of longitudinal sections of MWCNT fragments from samples S3 (Fig. 3, *a*) and S4 (Fig. 3, *b*). Both samples have a „Russian doll“ structure. The average outer diameter of nanotubes (the distance between the outermost stripes in the TEM image) was determined to be 18 nm, and the number of walls was 15.

In S3, the internal graphene layers are almost parallel to each other, and the average interlayer distance is ~ 3.45 Å. This distance increases to 3.6 Å in the three non-parallel surface layers. The crystalline structure of S4 (Fig. 3b) is significantly different from that of S3. The TEM image of S4 features darkened regions (indicated by red arrows) that correspond to distortions of graphene layers. The interlayer distances in darkened regions decrease to 3.3 Å. In

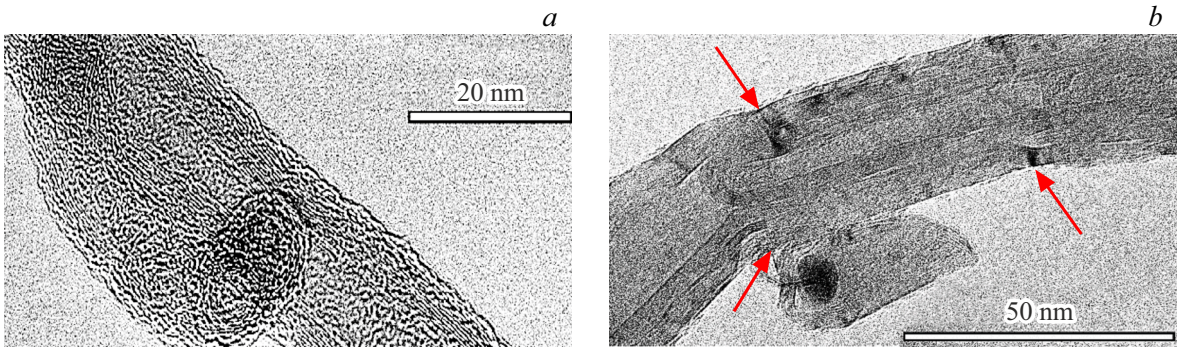

Figure 3. TEM image of MWCNTs with a diameter of 18 nm: *a* — sample S3; *b* — sample S4. Local deformation regions are denoted with red arrows.

the three upper layers, this distance varies from 3.0 to 3.8 Å. Analysis of the angles between layers reveals the growth of local deviations (to 15°–20° from the parallel). Similar changes were observed in flattened nanotubes and attributed to tensile, compression, shear, and torsional deformations (stacking disorder) [31,32].

Conclusion

The structure of MWCNTs with diameters of 7 nm (samples S1, S2) and 18 nm (samples S3, S4) was studied before and after grinding using the X-ray diffraction technique, Raman spectroscopy, TEM, and structural modeling.

The linear sizes of crystallites (determined from the I_D/I_G ratio) in samples S1 and S2 remained unchanged at 23 nm, while L_a in S4 decreased from 41 to 29 nm. The splitting of peak *G*- and shift of peaks *D*, *G*, and 2*D*- in S4 and the correspondence between the linear sizes of crystallites and a supercell of turbostratic graphene indicate that the angle of rotation of the upper layer regions is $\sim 10°$.

According to the TEM data, samples S3 and S4 have a „Russian doll“ structure. Compared to S3, sample S4 exhibits increased interlayer distances from 3.3 to 3.8 Å, relaxation of tensile and compressive stresses, and bending of the upper layers.

The XRD data revealed that the lattice parameters of samples S1 and S2 did not change after grinding. Compared to S3, sample S4 exhibits increased interlayer distances from 3.3 to 3.8 Å, relaxation of tensile and compressive stresses, and bending of the upper layers. The shift of peak (004) toward larger scattering angles is indicative of lattice parameter ***c*** reduction, while the splitting of peak (100) into four sub-peaks provides evidence of the formation of regions with four different hexagonal structures. These changes are also reflected in TEM images.

Thus, the combined use of experimental XRD, Raman spectroscopy, and TEM methods allows one to conduct an in-depth study revealing bending in mechanically processed MWCNTs and determine their effect on the mechanical state and structure of materials. The structural stability of 7 nm-diameter MWCNTs under mechanical stress makes them promising for use in composites, where preserving the original structure during interaction with composite components is crucial. In contrast, the increased surface area and orientational disorder of ground MWCNTs with a diameter of 18 nm open up opportunities for their application in catalytic processes and sensors that require active surfaces with a modifiable structure.

Funding

This study was carried out under the state assignment of the Institute of Strength Physics and Materials Science of the Siberian Branch of the Russian Academy of Sciences, project No. FWRW-2022-0002.

Acknowledgments

Equipment provided by the „Nanotech“ common use center of the Institute of Strength Physics and Materials Science was used in TEM studies.

Conflict of interest

The authors declare that they have no conflict of interest.

References

[1] M.F. Alif, R. Zainul, A. Mulyani, S. Syakirah, A. Zikri, A. Iqbal, M. Abdullah, A.A. Adeyi. Adv. J. Chem., Section A, **7**, 319 (2024). DOI: 10.48309/AJCA.2024.426290.1450
[2] K.K. Gangu, S. Maddila, S.B. Jonnalagadda. Sci. Total Environ., **646**, 1398 (2019). DOI: 10.1016/j.scitotenv.2018.07.375
[3] S. Kumar, H.K. Sidhu, A.K. Paul, N. Bhardwaj, N.S. Thakur, A. Deep. Sens. Diagn., **2**, 1390 (2023). DOI: 10.1039/d3sd00176h
[4] N. Anzar, R. Hasan, M. Tyagi, N. Yadav, J. Narang. Sens. Int., **1**, 100003 (2020). DOI: 10.1016/j.sintl.2020.100003
[5] Á. Kukovecz, T. Kanyó, Z. Kónya, I. Kiricsi. Carbon NY., **43**, 994 (2005). DOI: 10.1016/j.carbon.2004.11.030

[6] C. Vishal, S.K. Raju Chinthalapati, R. Krishna Kanala, R. Raman, R. Rao Bojja, R. Kanaparthi. Chemistry Select, **5**, 7031 (2020). DOI: 10.1002/slct.201904413
[7] S. Yang. Archit. Struct. Constr., **3**, 289 (2023). DOI: 10.1007/s44150-023-00090-z
[8] B. Xiang, R. Cheng, J. Zhu, Y. Zhou, X. Peng, J. Song, J. Wu. Sci. Rep., **13**, 16081 (2023). DOI: 10.1038/s41598-023-43133-7
[9] K. de Almeida Barcelos, J. Garg, D.C. Ferreira Soares, A.L.B. de Barros, Y. Zhao, L. Alisaraie. J. Drug Deliv. Sci. Technol., **87**, 104834 (2023). DOI: 10.1016/j.jddst.2023.104834
[10] F. Habeb Abdulrazzak, A. Fadel Alkiam, F. Hasan Hussein. In: Carbon Nanotubes, Intech. Open (2019). DOI: 10.5772/intechopen.85156
[11] W.H. Tan, S.L. Lee, C.T. Chong. Key Eng. Mater., **723**, 470 (2016). DOI: 10.4028/www.scientific.net/kem.723.470
[12] N. Bobenko, V. Egorushkin, A. Ponomarev. Nanomaterials (Basel), **12** (2022). DOI: 10.3390/nano12183139
[13] M.S. Dresselhaus, G. Dresselhaus, R. Saito, A. Jorio. Phys. Rep., **409**, 47 (2005). DOI: 10.1016/j.physrep.2004.10.006
[14] N.G. Bobenko, V.V. Shunaev, P.M. Korusenko, V.E. Egorushkin, O.E. Glukhova. Synth. Met., **307**, 117677 (2024). DOI: 10.1016/j.synthmet.2024.117677
[15] V.L. Kuznetsov, D.V. Krasnikov, A.N. Schmakov, K.V. Elumeeva. Phys. Status Solidi B Basic Res., **249**, 2390 (2012). DOI: 10.1002/pssb.201200120
[16] S.I. Moseenkov, A.V. Zavorin, A.V. Ishchenko, A.N. Serkova, A.G. Selyutin, V.L. Kuznetsov. J. Struct. Chem., **61**, 628 (2020). DOI: 10.1134/s0022476620040174
[17] L.G. Cançado, K. Takai, T. Enoki, M. Endo, Y.A. Kim, H. Mizusaki, A. Jorio, L.N. Coelho, R. Magalhães-Paniago, M.A. Pimenta. Appl. Phys. Lett., **88**, 163106 (2006). DOI: 10.1063/1.2196057
[18] D. Reznik, C.H. Olk, D.A. Neumann, J.R.D. Copley. Phys. Rev. B Condens. Matter, **52**, 116 (1995). DOI: 10.1103/physrevb.52.116
[19] A.V. Rozhkov, A.O. Sboychakov, A.L. Rakhmanov, F. Nori. Phys. Rep., **648**, 1 (2016). DOI: 10.1016/j.physrep.2016.07.003
[20] A.R. Stokes, A.J.C. Wilson. Proc. Phys. Soc., **56**, 174 (1944). DOI: 10.1088/0959-5309/56/3/303
[21] N. Bobenko, Y.A. Chumakov, A. Belosludtseva. Nanosci. Technol. Int. J., **13**, 67 (2022). DOI: 10.1615/nanoscitechnolintj.2022043261
[22] S. Zheng, Q. Cao, S. Liu, Q. Peng. J. Compos. Sci., **3**, 2 (2018). DOI: 10.3390/jcs3010002
[23] D. Fujita. Sci. Technol. Adv. Mater., **12**, 044611 (2011). DOI: 10.1088/1468-6996/12/4/044611
[24] R. Ishikawa, N.R. Lugg, K. Inoue, H. Sawada, T. Taniguchi, N. Shibata, Y. Ikuhara. Sci. Rep., **6**, 21273 (2016). DOI: 10.1038/srep21273
[25] L.G. Cançado, A. Jorio, E.H.M. Ferreira, F. Stavale, C.A. Achete, R.B. Capaz, M.V.O. Moutinho, A. Lombardo, T.S. Kulmala, A.C. Ferrari. Nano Lett., **11**, 3190 (2011). DOI: 10.1021/nl201432g
[26] A.V. Burenin. *Simmetriya kvantovoi vnutrimolekulyarnoi dinamiki* (Inst. Prikl. Fiz. Ross. Akad. Nauk, Nizhnii Novgorod, 2021), 4th ed. (in Russian).
[27] K.A. Bukunov, E.A. Vorobyeva, N.G. Chechenin. Moscow Univ. Phys. Bull., **77**, 50 (2022).
[28] I.S. Sokolov. Candidate's Dissertation in Mathematics and Physics (Kurchatovskii Inst., M., 2022) (in Russian).
[29] U. Mogera, G.U. Kulkarni. Carbon NY., **156**, 470 (2020). DOI: 10.1016/j.carbon.2019.09.053
[30] K. Kim, S. Coh, L.Z. Tan, W. Regan, J.M. Yuk, E. Chatterjee, M.F. Crommie, M.L. Cohen, S.G. Louie, A. Zettl. Phys. Rev. Lett., **108**, 246103 (2012). DOI: 10.1103/PhysRevLett.108.246103
[31] H.R. Barzegar, A. Yan, S. Coh, E. Gracia-Espino, C. Ojeda-Aristizabal, G. Cano-Márquez, L.F. Magana, M. Terrones, M. Endo, T. Hayashi. ACS Nano, **5**, 10591 (2011). DOI: 10.1021/nn204579p
[32] B. Xiang, J. Zhu, R. Cheng, Y. Zhou, Y. Xie, P. Zhou, J. Wu. Sci. Rep., **12**, 2 (2023). DOI: 10.1038/s41598-022-27005-3

Translated by T.Zorina